JACS
JOURNAL OF THE AMERICAN CHEMICAL SOCIETY

ARTICLE

pubs.acs.org/JACS

Reversible Photoinduced Twisting of Molecular Crystal Microribbons

Lingyan Zhu,[†] Rabih O. Al-Kaysi,[‡] and Christopher J. Bardeen*[,†]

[†]Department of Chemistry, University of California, Riverside, Riverside, California 92521, United States

[‡]Department of Basic Sciences, King Saud Bin Abdulaziz University for Health Sciences, National Guard Health Affairs, Riyadh 11423, Saudi Arabia

Supporting Information

ABSTRACT: 9-Anthracenecarboxylic acid, a molecule that undergoes a reversible [4 + 4] photodimerization, is prepared in the form of oriented crystalline microribbons. When exposed to spatially uniform light irradiation, these photoreactive ribbons rapidly twist. After the light is turned off, they relax back to their original shape over the course of minutes. This photoinduced motion can be repeated for multiple cycles. The final twist period and cross-sectional dimensions of individual microribbons are measured using a combination of atomic force and optical microscopies. Analysis of this data suggests that the reversible twisting involves the generation of interfacial strain within the ribbons between unreacted monomer and photoreacted dimer regions, with an interaction energy on the order of 3.4 kJ/mol. The demonstration of reversible twisting without the need for specialized irradiation conditions represents a new type of photoinduced motion in molecular crystals and may provide new modes of operation for photomechanical actuators.

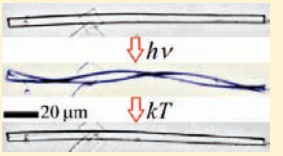

INTRODUCTION

The transformation of photon energy into mechanical work is interesting from both fundamental and practical standpoints. Photons provide a versatile and easily controllable energy source for various types of nanoscale machines.[1] Liquid crystal elastomers are a widely studied class of materials whose combination of flexibility and molecular order allows them to undergo large deformations after exposure to light.[2−7] Their photomechanical response arises from the photoisomerization of a reactive molecule incorporated into the liquid crystal polymer, usually an azobenzene derivative. More highly ordered molecular crystals have also been shown to undergo photoinduced bending and expansion, with the potential advantages of greater Young's moduli and faster response times.[8−16] Chemical reactions in crystals are complicated by the need to consider the role of the crystal environment in modulating the production of new chemical species.[17−19] How the presence of those new chemical species influences the overall crystal structure is less studied. For macroscopic molecular crystals, photochemical reactions often lead to phase separation between reacted and unreacted regions that shatter the crystal.[20] For smaller crystals with large surface-to-volume ratios, the buildup of interfacial stress between reacted and unreacted domains can be alleviated at a nearby surface, rather than by generating a fracture.[21,22] The robustness of ultrasmall crystals permits a much wider variety of photochemical systems to be used in photomechanical structures. Our group has studied the photomechanical response of organic molecular crystal micro- and nanostructures as a general approach for making photoresponsive objects.[23−26] The photochemical reaction used to transform light into mechanical motion is the concerted [4 + 4] cyclodimerization reaction of two anthracene chromophores. Steric repulsion due to the atypical "head-to-head" packing makes this reaction reversible in crystalline 9-anthracenecarboxylic acid (9AC),[27] as shown in Scheme 1. Note that in Scheme 1, some 9AC molecules are "left out" of the photodimerization reaction due to statistical considerations. This mix of reacted and unreacted molecules is unique to crystals containing one-dimensional stacks and is vital for interpreting the experimental results in this Article. We have previously demonstrated that crystalline nanorods composed of 9AC could undergo reversible bending driven by strain generated between photoreacted and unreacted regions of the rod.[26] This phenomenon does not rely on generating a gradient of reacted molecules along the direction of the bend, as in many polymer actuators,[28,29] and allowed us to demonstrate controlled, reversible bending in 9AC molecular crystal nanorods with diameters as small as 35 nm.[26]

The previously studied nanorod bending required the selective illumination of a single point or segment of the rod. We became interested in whether other types of photoactivated motions could be induced, especially under conditions of spatially uniform irradiation. In this Article, we describe a different morphology of 9AC crystals, microribbons, that undergoes reversible twisting under uniform illumination. The twist period is controlled by the amount of light exposure and saturates at a value that depends on the cross section of the ribbon. The twist relaxes over the course of minutes, consistent with the dissociation of the dimer 9AC back into its monomeric form.[23,26] Using a combination of atomic force and optical microscopies, the twist period has been measured as a function of ribbon cross section. We find that the mechanism of the twisting is consistent with stress induced by the presence of two incommensurate chemical species. In the 9AC system, these two species are most likely the

Received: March 2, 2011
Published: July 12, 2011

Scheme 1. [4 + 4] Photodimerization and Dissociation Reaction Scheme of 9AC along a Single Crystal Stack

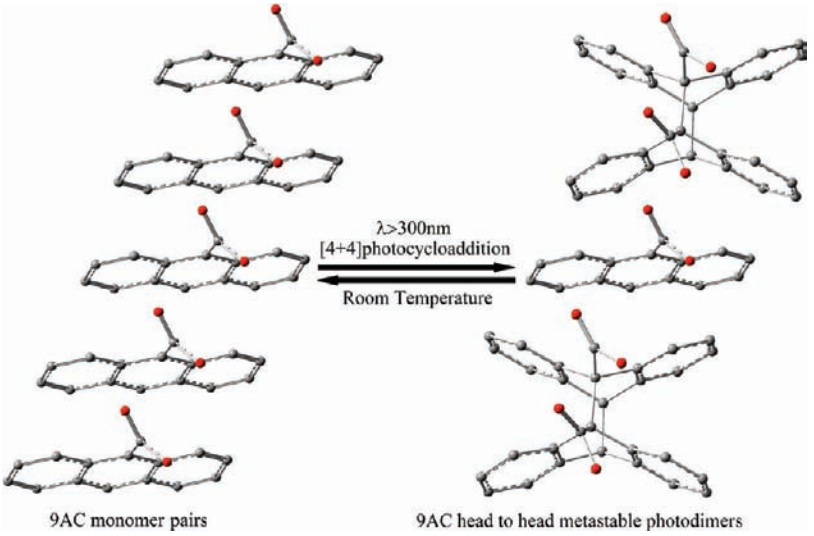

photoreacted dimers and the unreacted monomers left over due to the statistical nature of the dimerization reaction. The reversible generation of a photoinduced twist in crystalline microribbons represents a new class of motions accessible through solid-state photochemistry and also provides a new way to induce large deformations without asymmetric or structured illumination conditions. The ability to induce repeated twisting in such small objects may make them useful for powering small-scale machines.

EXPERIMENTAL SECTION

1. Preparation of Crystalline Ribbons. All of the 9AC microribbons were prepared by the floating drop method.[30] 1.9 mg of 9AC (TCI, >97%) was dissolved in 1.0 mL of filtered ethyl acetate (Sigma, 99.5+%), and then this solution was slowly added to the surface of MilliQ Millipore purified H_2O in a Petri dish (VWR, 60 × 15 mm). The Petri dish was covered and left in the dark for 48 h. During this time, as the solvent evaporated, the 9AC slowly crystallized out as ribbons floating on the water surface.

2. Powder X-ray Diffraction (XRD) Measurements. When a dry sample of microribbons was deposited on a microscope slide, a range of ribbon orientations was obtained. To ensure that the majority of 9AC ribbons ended up lying flat (wide axis parallel to the substrate surface), a concentrated solution of ribbons floating in H_2O was first placed on a glass slide and then slowly dried. The drying could be accomplished either by slow evaporation or by carefully using a Kimwipe to wick away the excess water underneath the floating ribbons. Powder X-ray diffraction data were collected on a Bruker D8 Advance X-ray powder diffractometer (CuK radiation, λ = 1.5418 Å, 40 kV/40 mA power) at room temperature.

3. Scanning Electron Microscopy (SEM) Measurements. For SEM measurements, a drop of 9AC ribbons in MilliQ H_2O water was placed on a microscope coverslip that was affixed to a piece of conducting copper tape mounted on a SEM stub. The water was gently evaporated under vacuum, leaving behind dispersed bundles of ribbons. The SEM stub was placed in a sputter coater (Cressington 108 Auto) and coated with Pt/Au for 40 s. The SEM stub was then placed inside a scanning electron microscope (XL30-FEG) for imaging.

4. Atomic Force Microscopy (AFM) Measurements. For AFM measurements, dried samples were prepared in the same way as for the XRD experiments. To examine the topology of single ribbons, a Novascan AFM mounted on top of an Olympus IX-70 inverted fluorescence microscope was used. The AFM was calibrated in x, y, and z directions before the measurements. An intermittent contact mode scan was performed with a scan rate of 1 Hz, scan resolution of 400 × 400, and scan size of 73 × 73 μm. Individual ribbons were illuminated with 410 nm light from a Hg lamp, and then optically imaged to determine the twist period. After the ribbon relaxed back to its untwisted state, it was scanned with the AFM to determine its width and height.

5. Optical Microscopy Measurements. To prepare aqueous samples of 9AC microribbons, a few drops of 50% H_3PO_4 were added to MilliQ H_2O containing 9AC ribbons to prevent H_2O evaporation during the measurements. We use H_3PO_4 because our previous work on molecular crystal nanorods has shown that it is compatible with crystalline 9AC and does not change the hydrogen bonding of the carboxylic acid groups within the crystal. The presence of H_2O and H_3PO_4 does not play any role in the observed twisting, because this motion also occurs in ribbons on dry surfaces. A drop of the acidic solution of 9AC ribbons was transferred to a microscope slide and then covered with a microscope coverslip. To measure the dynamic process of 9AC ribbons untwisting, 9AC ribbons were first irradiated by 440 nm light (~20 mW/mm^2) for a few seconds and then imaged in transmission using a 40× 0.6 NA objective and visible light. Images were captured by a DCM300 digital camera to record the untwisting.

RESULTS AND DISCUSSION

9AC crystals can grow in a variety of shapes and sizes, but the most commonly observed morphologies are ribbons and needles. After some experimentation, we found that the growth of microribbons could be maximized by making use of very flat growth surfaces, and our yields of microribbons were highest when the floating drop method was used with the solvent ethyl acetate. In general, all growth methods produced a distribution of microribbon lengths and cross sections. The rectangular cross section of the microribbons can be seen in the SEM images in Figure 1, as well as the distribution of lengths (l), widths (w), and thicknesses (h). The crystalline nature of the microribbons was confirmed by powder XRD measurements. 9AC crystallizes in columns of π-stacked anthracene moieties, where each column is connected to a neighboring column through intermolecular hydrogen bonds between opposing carboxylic acid groups.

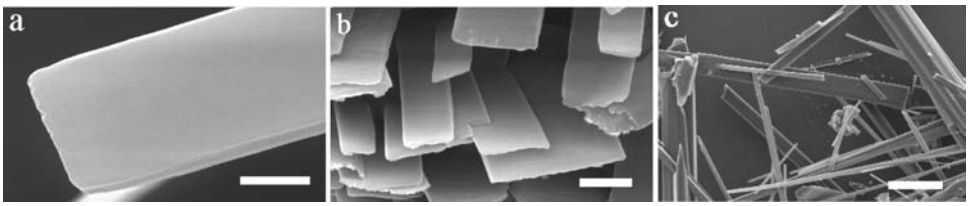

Figure 1. SEM images of 9-AC ribbons of different sizes: (a) scale bar is 2 μm; (b) scale bar is 1 μm; and (c) scale bar is 25 μm.

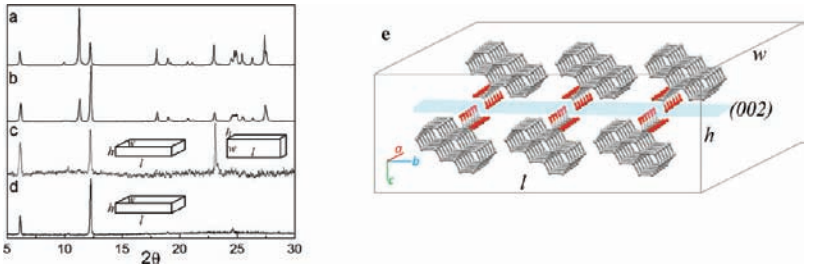

Figure 2. X-ray powder diffraction patterns for 9AC: (a) Calculated pattern of monoclinic 9AC; (b) experimental pattern of powdered 9AC crystals; (c) pattern of ribbons randomly deposited on the surface as shown in the inset cartoon, with the three peaks corresponding to parallel planes (002) and (004), and the almost perpendicular (101) plane; (d) pattern of ribbons lying flat on the surface as shown in the inset cartoon, with the two peaks corresponding to parallel planes (002) and (004) being most prominent; and (e) side view of the 9AC crystal packing within the microribbon, looking along the long axis. Note that for ribbons $h < w$.

In Figure 2a, we show the calculated powder XRD pattern obtained from the monoclinic single crystal structure. Figure 2b shows the experimental powder XRD of the powdered microribbons. The peak positions and overall shape of this pattern agree well with the calculated pattern in Figure 2a, but there are some discrepancies in the peak intensities. These discrepancies are most likely due to residual orientation in the powdered sample arising from the tendency of 9AC crystals to form rods or ribbons that lie flat on the substrate, as discussed below. Figure 2c shows the powder XRD pattern for intact microribbons that have been dried and randomly deposited onto a flat substrate. When the powder XRD pattern of this sample is measured, three major peaks are seen, corresponding to the 002 Miller plane at $2\theta = 6.13°$, the 004 plane at $2\theta = 12.21°$, and the 101 Miller plane at $2\theta = 23.09°$. The first two planes are parallel and extend between stacks of 9AC molecules, as shown in Figure 2e, while the 101 Miller plane makes an angle of 81.57° with respect to the 002 plane. In contrast, when the sample is carefully dried on the substrate, inspection using optical microscopy reveals that the majority of these ribbons lie flat on the surface, with their short axis pointing up (as illustrated in Figure 2d). We then obtain the powder XRD pattern in Figure 2d, which is dominated by the 002 and 004 peaks. The much smaller peak at $2\theta = 24.62°$ corresponds to the 008 Miller plane, also parallel to the 002 and 004 planes. In addition to these two dominant peaks, another very small peak at $2\theta = 10.34°$ is also observed in Figure 2c, corresponding to a small triclinic component within the largely monoclinic ribbons.[31] If we assume that the pattern in Figure 2c arises from a combination of ribbons lying on edge and lying flat, while that in Figure 2c arises from only ribbons that lie flat, then we can determine the absolute orientation of the crystal within the ribbon. The crystal orientation consistent with the data in Figure 2c and d has the 002 plane perpendicular to h and the 101 plane perpendicular to w, as shown in Figure 2e. It should be noted that the c-axis of the unit cell is aligned almost parallel to the height (h) of the ribbon, while the ab plane is parallel to the plane defined by the width (w) and length (l) of the ribbon. The stacks of 9AC monomers extend across the width of the ribbon.

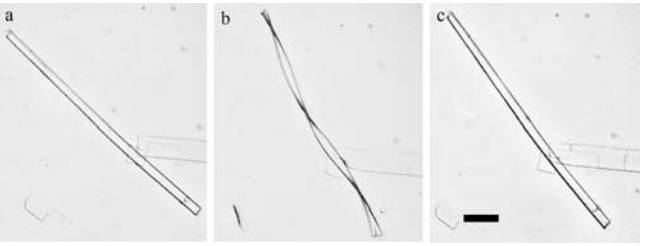

Figure 3. Optical microscopy images of a 9AC ribbon's reversible twisting behavior: (a) before irradiation; (b) immediately after irradiation; and (c) 9AC belt recovered after 9 min in the dark; the scale bar is 20 μm. Note that the 9AC ribbon on the bottom right of the frame has a larger width and fractures when exposed to the UV light.

We initially expected the microribbons to bend under localized photoexcitation but to retain their overall shape under uniform photoexcitation, similar to what was observed previously in 9AC nanorods. Instead, under uniform lamp irradiation, we observed a dramatic twisting behavior, as illustrated in Figure 3. Under either 410 or 440 nm irradiation, a straight ribbon would rapidly twist over its entire length, while the intense green-yellow fluorescence disappeared, indicating that a photochemical reaction was consuming the 9AC molecules. No twisting or fluorescence decrease was observed for irradiation at wavelengths greater than 600 nm, ruling out a heating effect or phonon-mediated mechanism. The twisting could be observed in 25−80% of the ribbons, depending on the sample. The ribbons twisted more easily when suspended in an aqueous solution than on a dry surface. The reason for this may lie in increased surface adhesion in the dry samples. Larger crystals would often break into segments during this process, but ribbons with widths on the order of 20 μm or less were remarkably robust. In general, the twist period (L_{twist} = the distance required for the ribbon to

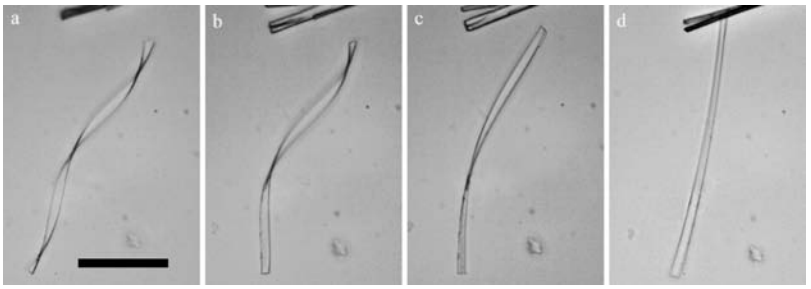

Figure 4. Optical microscopy images of the slow untwisting of 9AC ribbons after the irradiation is turned off. Time interval between images: (a) immediately after exposure; (b) 3 min later; (c) 4.5 min later; and (d) 11.5 min later. The scale bar is 50 μm.

undergo a full 2π rotation) was larger for larger ribbons (Supporting Information Figure S1). After the UV light was turned off, the twisted ribbon continued to twist for 2−4 min. Eventually, the twisting would stop and then reverse, the ribbon untwisting until it returned to its previous straight shape over the course of 5−15 min. This straightening process was 2−4 times slower than the rate of fluorescence recovery and nanorod unbending observed previously in 9AC nanorods.[23,26] During the relaxation, the twist period changes continuously, as shown in the sequence of images in Figure 4. After the ribbon had returned to its original shape, the process could be repeated multiple times until the ribbon either broke or photobleached. The direction of each sequential twist for a given ribbon was random after each irradiation period (Supporting Information Figure S2). For some ribbons, we observed that prolonged (minutes) light exposure leads to untwisting instead of a stable twisted structure. The origin of this behavior is discussed below.

Quasi-periodic twisting in crystals, as seen in Figures 3 and 4, can arise from several distinct mechanisms. To investigate the mechanism of twisting and the variability in twist period, we used AFM to measure the cross-sectional profile of ribbons that exhibited twisting. Although we were unable to measure the cross section of a twisted ribbon, we do not expect it to be significantly different from that of the untwisted ribbon, because prior measurements on photoreacted nanorods of 9AC showed less than a 3% change in length and diameter.[23] In general, the cross section of a ribbon is not a perfect rectangle with well-defined h and w values. We chose to parametrize the cross section in two ways. First, we simply integrate over the entire AFM profile to obtain a single quantity, the cross-sectional area S, that contains no information about the detailed shape. Second, to take into account the detailed shape of the ribbons, we extracted values for the height h and width w by defining the profile height at the center of the profile to be h and then taking the full width at $h/2$ to be w. An example of this measurement is given in Figure 5, along with an illustration of how h, w, and L_{twist} were determined. Note that we were limited in the size range we could examine: larger ribbons tend to fracture under illumination (Supporting Information Figure S3), while smaller ones had twist periods that were difficult to resolve using our optical microscopy setup. Additional details along with a table of h and w values for all ribbons examined by AFM are given in the Supporting Information, Figures S4−S6 and Table 1.

Measurements of S, h, w, and L_{twist} allow us to examine the mechanism of the twisting. Static twisted organic molecular crystals are relatively rare,[32,33] and most instances have been interpreted in terms of a theory by Eshelby that explained the twist in terms of a propagating screw dislocation at the center of a

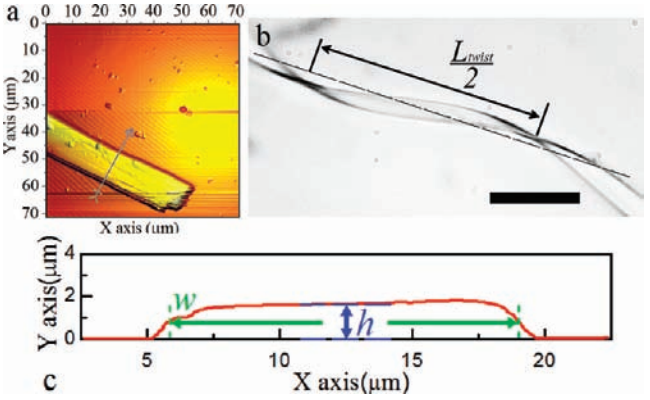

Figure 5. (a) AFM (atomic force microscopy) images of 9AC crystalline ribbon; (b) optical mcroscopy image of a twisted ribbon, the scale bar is 20 μm; and (c) scheme to extract height (h) and width (w) of the ribbon from the AFM profile curve: h was extracted from the center profile height; w was the full width at half height. The ribbons shown in (a) and (b) are different.

crystal rod.[34,35] Frank showed that if this screw dislocation is larger than a few lattice spacings, a void or pipe must form at the center of the crystal, parallel to the direction of twist propagation along l, with a giant Burgers vector associated with it.[36] Both types of screw-dislocation theories are valid for a single-component system and predict that the twist period L_{twist} should depend linearly on the cross-sectional area S:

$$L_{twist} = 2\pi k\frac{S}{b} \quad (1)$$

where k is a constant on the order of unity and b is the magnitude of the Burgers vector associated with the screw-dislocation defect. Figure 6a shows a fit to our data using eq 1, yielding a straight line with a slope of 12 and a relatively poor R^2 value of 0.76. It is clear from the residuals in Figure 6a that the fit systematically underestimates the amount of twist for smaller cross-section ribbons in particular. If we set $k = 1$, we can extract a value for b = 0.51 μm. This large value of b places our microribbons in the Frank regime, but our optical microscopy images provide no evidence for the formation of a void during the crystal twisting process. Given the value of b obtained experimentally, we can estimate the diameter D of the pipe using the following equation:[37,38]

$$D = \frac{Gb^2}{4\pi^2\gamma} \quad (2)$$

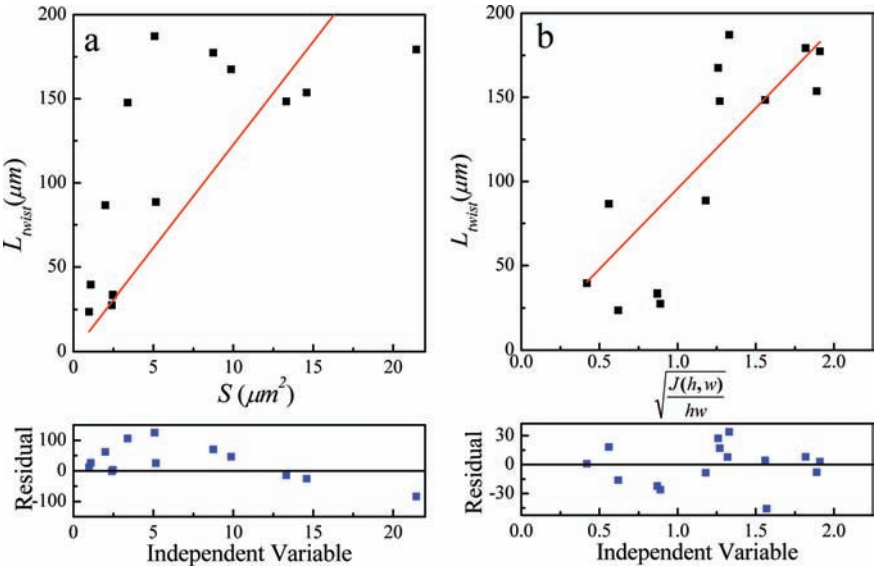

Figure 6. (a) Linear fit of twist period L_{twist} versus cross-section area ($S = hw$) according to Eshelby theory as given by eq 1. The R^2 value is 0.76, and slope is 12. (b) Linear fit of twist period L_{twist} versus $((J(h,w))/hw)^{1/2}$ as given by eq 5. The R^2 value is 0.93, and slope is 96.

where G is the shear modulus and γ is the surface energy. Typical values for organic molecular crystals are $G = 5$ GPa[39,40] and $\gamma = 0.2$ J/m^2,[41,42] leading to a value of $D > 150$ μm for $b = 0.51$ μm. This value of D is greater than the width of our microribbons. Even given the uncertainties in our estimate of D, any formation of a micrometer-scale hollow pipe within our ribbons should be easily observable by optical microscopy. The poor quality of the linear fit, coupled with the lack of the void formation necessary to explain the giant b value, suggest that the simple screw-dislocation mechanism is not operative in our twisted ribbons.

A second mechanism to explain crystal twisting involves strain energy that builds up due to the interaction between two different chemical species in a single crsytal. This type of mechanism has been invoked to explain twisting in polymer spherulites[43−45] and is sometimes referred to as "heterometry".[46] The interaction can occur between the host molecule and a chemically distinct impurity, as seen in some minerals,[47,48] or between reacted and unreacted forms of the same molecule.[49] We now consider whether chemically reasonable interaction energies can cause the observed twisting of our 9AC microribbons. For a rectangular cross-section ribbon of width w and height h, as shown in Figure 2d, the energy density per unit volume W required to generate a twist $(\partial\theta/\partial x)$ (in radians per unit length) is given by[44]

$$W(h,w) = \frac{G \cdot J(h,w)\left(\frac{\partial\theta}{\partial x}\right)^2}{hw} \tag{3}$$

where G is the shear modulus and $J(h,w)$ is the torsional constant of the ribbon. The function $J(h,w)$ is rigorously given by an infinite sum.[44,50] We found that only the first two terms of the sum had to be retained for an accurate calculation of $J(h,w)$ given the range of experimental h and w values:

$$J(h,w) \cong h^3 w\left[\frac{1}{3} - \frac{64}{\pi^5}\frac{h}{w}\tanh\left[\frac{\pi w}{2h}\right]\right] \tag{4}$$

If we rearrange eq 3, solve for $(\partial\theta/\partial x)$, and then integrate over a single period of twist (i.e., $\theta = 2\pi$), we obtain an expression for the period L_{twist} as a function of h and w:

$$L_{twist} = 2\pi\sqrt{\frac{G}{W}}\sqrt{\frac{J(h,w)}{hw}} \tag{5}$$

Both G and W are unknown for the 9AC crystal. If we assume that W attains a maximum value after irradiation and then remains constant, and is the same for all of the ribbons (see discussion below), then eq 5 predicts that a plot of L_{twist} versus $((J(h,w))/hw)^{1/2}$ should be linear, as shown in Figure 6b. The R^2 value for a linear fit to this data is 0.93, significantly better than that obtained using eq 1. The more uniform scatter of the data points above and below the fit line also results in better residuals and more confidence in this fitting model. The slope and R^2 values are robust with respect to the method used to extract h and w values from the AFM data (Supporting Information, Figure S7). The slope of the fit line in Figure 6b is 96, which from eq 5 should equal $2\pi(G/W)^{1/2}$. Assuming a typical value of $G = 5$ GPa, and the concentration of 9AC in the crystal as 6.3 M, we obtain $W = 3.4$ kJ/mol at the maximum photoconversion. This calculated energy density W falls within the range expected for noncovalent interactions between different molecules, indicating that this analysis leads to chemically reasonable values. Note that if the calculated value for W had fallen outside this range, we would have to consider other types of energy contributions in addition to intermolecular interactions.

In previous studies of heterometry-induced twisting, the two different chemical species were supplied by the environment. In our case, second chemical species must be reversibly generated in situ by the photochemical reaction. The most logical candidates for the two interacting species are the monomeric and dimeric forms of 9AC. When a dimerization reaction occurs within a stack of monomers, statistical considerations make it impossible to react 100% of the 9AC molecules, even under continuous illumination. Theoretically, at least 13% of the monomers were left out of the reaction,[51,52] although recent studies indicate that this fraction is closer to 25% for 9AC.[53] This fraction of unreacted 9AC monomers comprises the second species needed to generate strain and drive the twisting without

the need for tailored illumination conditions. In addition to the better fit to the data in Figure 6b, there is further evidence for this mechanism. One factor that suggests that the twisting results from dynamic monomer and dimer domain formation is the random twist direction after each irradiation period. If the twisting relied on the presence of static structural or chemical defects, then they would be expected to initiate the same twist direction each time, contrary to what is observed. An additional piece of evidence in favor of this mechanism is that the linear slope in Figure 6b shows that W, the energy density, is the same for all ribbons after prolonged light exposure. If the energy is proportional to the concentration of the unreacted monomers, then this constant W implies a constant fraction of "left-over" monomeric 9AC molecules, as predicted theoretically. If we assume that the interaction energy W results from the interaction of 25% of the total monomers (i.e., the minimum number left unreacted), then the actual interaction energy is approximately 13 kJ per mole of unreacted monomer. We may speculate that the strain energy W arises from the disruption of the intrastack hydrogen-bond network due to the presence of monomer regions that are not aligned with neighboring dimer stacks. It is important to point out that the photoinduced heterometry mechanism relies on the statistical nature of the 9AC photoreaction that prevents 100% conversion of the monomer into dimers, making the twisting an intrinsic property of the 9AC microribbons.

If we assume that the unreacted monomers are randomly distributed throughout the dimer crystal, they would have to migrate to form phase segregated regions that would give rise to the interfacial strain energy. The photodimerization of 9AC is associated with a disorder increase in the lattice,[53] which could facilitate such migration. Molecular migration would also explain both the continued twisting that is observed after the light is turned off and the fact that the shape recovery is slower than the measured time for fluorescence recovery or nanorod unbending in 9AC. However, molecular migration over long distances is difficult in the absence of cooperative effects and would be energetically costly.[54] A second explanation for the delayed response is that localized regions of monomers and dimers are formed during the photoreaction by exciton trapping at defect sites or stress points.[55,56] In this scenario, the time-lag between the light exposure and the completion of the physical motion would be a mechanical effect resulting from slow lattice relaxation rather than molecular migration. The relative importance of molecular translation as opposed to larger scale mechanical effects in the crystal for determining the overall time response of the twisting remains to be determined.

Lastly, we contrast the ribbon twisting described in this Article with the nanorod bending observed in our previous work. Previously, we have observed reversible bending for 9AC nanorods using spatially localized one-photon[23] and two-photon excitation.[26] We attributed the bending to local strain created at the interface between reacted and unreacted crystal regions along the nanorod. When the rods were uniformly illuminated, no interfaces were created and no bending was observed, only a slight expansion.[23] At first glance, the twisting seen here appears to be different from the bending observed earlier. Yet Eshelby realized that a bend can be thought of as a partial twist.[34] Indeed, illumination of a short segment of a ribbon gives rise to a partial twist that looks like a bend. Direct comparison of the two morphologies is complicated by their different crystal orientations (the long axis of the rods corresponds to the crystal c-axis, which is perpendicular to the long axis of the ribbons as shown in Figure S8 of the Supporting Information) and different aspect ratios (h and w are approximately equal for the cylindrical nanorods as opposed to $w/h > 2$ for the microribbons). Nevertheless, it is likely that the same physical process underlies both types of motion.

CONCLUSION

The data in this Article demonstrate a new mode of reversible photomechanical deformation in molecular crystals. Microribbons consisting of oriented 9AC crystals undergo reversible twisting motions without the need for specialized irradiation conditions, like focused light or controlled polarization. The time-dependent relaxation of the twist period and its dependence on the cross-sectional dimensions of the ribbon are both consistent with a mechanism based on internal strain generated by the coexistence of regions composed of dimeric and monomeric 9AC. The twisting motion is specific to a single crystal morphology and size range: if the cross-sectional area of a ribbon is too large, it will fracture rather than twist. Because the twisting is an intrinsic crystal property, it should be manifested by much smaller structures that share the same ribbon morphology. It should also be insensitive to the illumination conditions as long as photons can reach the crystal and induce the [4 + 4] photocyclization reaction. This work provides a further illustration of the surprising versatility of molecular crystals as photoresponsive systems and suggests that control of molecular crystal shape and size may prove to be a fruitful way to design systems with improved photomechanical properties.

ASSOCIATED CONTENT

Supporting Information. Figures for size dependence of twisting period; images of reversible twisting with random twisting direction; images of larger ribbons shatter upon illumination; AFM (atomic force microscope) profile images of 9AC ribbons; integration cross-section areas of the ribbons for Eshelby's theory; linear fitting according to "heterometry" with a different extraction method of h and w, along with extraction schemes; fluorescence microscopy images for different twisting ribbons; table with all of the parameters for linear fitting; and orientation of 9AC crystalline nanorods. This material is available free of charge via the Internet at http://pubs.acs.org.

AUTHOR INFORMATION

Corresponding Author
christopher.bardeen@ucr.edu

ACKNOWLEDGMENT

This research was supported by the National Science Foundation, grant DMR-0907310. The electron microscopy measurements were done at the Center for Advanced Materials and Microscopy (CFAMM) at UC Riverside. R.O.A.-K. acknowledges the support of KSAU-HS/KAIMRC through grants RC08/093 and RC10/104.

REFERENCES

(1) Ballardini, R.; Balzani, V.; Credi, A.; Gandolfi, M. T.; Venturi, M. *Acc. Chem. Res.* **2001**, *34*, 445–455.

(2) Ikeda, T.; Mamiya, J.; Yu, Y. *Angew. Chem., Int. Ed.* **2007**, *46*, 506–528.

(3) White, T. J.; Tabiryan, N. V.; Serak, S. V.; Hrozhyk, U. A.; Tondiglia, V. P.; Koerner, H.; Vaia, R. A.; Bunning, T. J. *Soft Matter* **2008**, *4*, 1796–1798.
(4) Yu, Y.; Nakano, M.; Ikeda, T. *Nature* **2003**, *425*, 145.
(5) Oosten, C. L. v.; Bastiaansen, C. W. M.; Broer, D. J. *Nat. Mater.* **2009**, *8*, 677–682.
(6) Finkelmann, H.; Nishikawa, E.; Pereira, G. G.; Warner, M. *Phys. Rev. Lett.* **2001**, *87*, 015501/1–015501/4.
(7) Camacho-Lopez, M.; Finkelmann, H.; Shelley, P. P.-M. *Nat. Mater.* **2004**, *3*, 307–310.
(8) Boldyreva, E. V.; Sinelnikov, A. A.; Chupakhin, A. P.; Lyakhov, N. Z.; Boldyrev, V. V. *Dokl. Akad. Nauk USSR* **1984**, *277*, 893–896.
(9) Lange, C. W.; Foldeaki, M.; Nevodchikov, V. I.; Cherkasov, V. K.; Abakumov, G. A.; Pierpont, C. G. *J. Am. Chem. Soc.* **1992**, *114*, 4220–4222.
(10) Koshima, H.; Ojima, N.; Uchimoto, H. *J. Am. Chem. Soc.* **2009**, *131*, 6890–6891.
(11) Naumov, P.; Kowalik, J.; Solntsev, K. M.; Baldridge, A.; Moon, J.-S.; Kranz, C.; Tolbert, L. M. *J. Am. Chem. Soc.* **2010**, *132*, 5845–5857.
(12) Kobatake, S.; Takami, S.; Muto, H.; Ishikawa, T.; Irie, M. *Nature* **2007**, *446*, 778–781.
(13) Flannigan, D. J.; Samartzis, P. C.; Yurtsever, A.; Zewail, A. H. *Nano Lett.* **2009**, *9*, 875–881.
(14) Colombier, I.; Spagnoli, S.; Corval, A.; Baldeck, P. L.; Giraud, M.; Leaustic, A.; Yu, P.; Irie, M. *J. Chem. Phys.* **2007**, *126*, 011101/1–011101/3.
(15) Uchida, K.; Sukata, S.; Matsuzawa, Y.; Akazawa, M.; Jong, J. J. D. d.; Katsonis, N.; Kojima, Y.; Nakamura, S.; Areephong, J.; Meetsma, A.; Feringa, B. L. *Chem. Commun.* **2008**, 326–328.
(16) Morimoto, M.; Irie, M. *J. Am. Chem. Soc.* **2010**, *132*, 14172–14178.
(17) McBride, J. M.; Segmuller, B. E.; Hollingsworth, M. D.; Mills, D. E.; Weber, B. A. *Science* **1986**, *234*, 830–835.
(18) Luty, T.; Eckhardt, C. J. *J. Am. Chem. Soc.* **1995**, *117*, 2441–2452.
(19) MacGillivray, L. R.; Papaefstathiou, G. S.; Friscic, T.; Hamilton, T. D.; Bucar, D. K.; Chu, Q.; Varshney, D. B.; Georgiev, I. G. *Acc. Chem. Res.* **2008**, *41*, 280–291.
(20) Keating, A. E., Garcia-Garibay, M. A. *Organic and Inorganic Photochemistry*; Ramamurthy, V., Schanze, K. S., Eds.; Marcel Dekker: New York, 1998.
(21) Bucar, D. K.; MacGillivray, L. R. *J. Am. Chem. Soc.* **2007**, *129*, 32–33.
(22) Takahashi, S.; Miura, H.; Kasai, H.; Okada, S.; Oikawa, H.; Nakanishi, H. *J. Am. Chem. Soc.* **2002**, *124*, 10944–10945.
(23) Al-Kaysi, R. O.; Bardeen, C. J. *Adv. Mater.* **2007**, *19*, 1276–1280.
(24) Al-Kaysi, R. O.; Dillon, R. J.; Zhu, L.; Bardeen, C. J. *J. Colloid Interface Sci.* **2008**, *327*, 102–107.
(25) Al-Kaysi, R. O.; Muller, A. M.; Bardeen, C. J. *J. Am. Chem. Soc.* **2006**, *128*, 15938–15939.
(26) Good, J. T.; Burdett, J. J.; Bardeen, C. J. *Small* **2009**, *5*, 2902–2909.
(27) Ito, Y.; Fujita, H. *J. Org. Chem.* **1996**, *61*, 5677–5680.
(28) Dunn, M. L. *J. Appl. Phys.* **2007**, *102*, 013506/1–013506/7.
(29) Warner, M.; Mahadevan, L. *Phys. Rev. Lett.* **2004**, *92*, 134302/1–134302/4.
(30) Campione, M.; Ruggerone, R.; Tavazzi, S.; Moret, M. *J. Mater. Chem.* **2005**, *15*, 2437–2443.
(31) Heller, E.; Schmidt, G. M. J. *Isr. J. Chem.* **1971**, *9*, 449–462.
(32) McClellan, A. L. *J. Chem. Phys.* **1960**, *32*, 1271–1272.
(33) Kawabata, K.; Kumagai, T.; Mizutani, M.; Sambongi, T. *J. Phys. I France* **1996**, *6*, 1575–1580.
(34) Eshelby, J. D. *J. Appl. Phys.* **1953**, *24*, 176–179.
(35) Schultz, J. M.; Kinloch, D. R. *Polymer* **1969**, *10*, 271–278.
(36) Frank, F. C. *Acta Crystallogr.* **1951**, *4*, 497–501.
(37) Si, W.; Dudley, M.; Glass, R.; Tsvetkov, V.; Carter, C. *J. Electron. Mater.* **1997**, *26*, 128–133.
(38) Jacobs, B. W.; Crimp, M. A.; McElroy, K.; Ayres, V. M. *Nano Lett.* **2008**, *8*, 4353–4358.
(39) Capaldi, F. M.; Boyce, M. C.; Rutledge, G. C. *J. Chem. Phys.* **2006**, *124*, 214709/1–214709/4.
(40) Roberts, R. J.; Rowe, R. C.; York, P. *Powder Technol.* **1991**, *65*, 139–146.
(41) Engkvist, O.; Price, S. L.; Stone, A. J. *Phys. Chem. Chem. Phys.* **2000**, *2*, 3017–3027.
(42) Nabok, D.; Puschnig, P.; Ambrosch-Draxl, C. *Phys. Rev. B* **2008**, *77*, 245316/1–245316/4.
(43) Calvert, P. D.; Uhlmann, D. R. *J. Polym. Sci.* **1973**, *11*, 457–465.
(44) Schultz, J. M. *Polymer* **2003**, *44*, 433–441.
(45) Lotz, B.; Cheng, S. Z. D. *Polymer* **2005**, *46*, 577–610.
(46) Shtukenberg, A.; Punin, Y. *Optically Anomalous Crystals*; Springer: Dordrecht, Netherlands, 2007.
(47) Wang, Y.; Merino, E. *Am. J. Sci.* **1995**, *295*, 49–77.
(48) Comer, J.; Ortoleva, P. *Am. Mineral.* **2007**, *92*, 1952–1957.
(49) Shtukenberg, A. G.; Freudenthal, J.; Kahr, B. *J. Am. Chem. Soc.* **2010**, *132*, 9341–9349.
(50) Barber, J. R. *Elasticity*; Kluwer: Dordrecht, Netherlands, 2002.
(51) Cohen, E. R.; Reiss, H. *J. Chem. Phys.* **1963**, *38*, 680–691.
(52) Even, J.; Bertault, M. *J. Chem. Phys.* **1999**, *110*, 1087–1096.
(53) More, R.; Busse, G.; Hallmann, J.; Paulmann, C.; Scholz, M.; Techert, S. *J. Phys. Chem. C* **2010**, *114*, 4142–4148.
(54) Atwood, J. L.; Barbour, L. J.; Jerga, A.; Schottel, B. L. *Science* **2002**, *298*, 1000–1002.
(55) Schipper, P. E.; Walmsley, S. H. *Proc. R. Soc. London, Ser. A* **1976**, *348*, 203–219.
(56) Suzuki, M.; Iida, T.; Nasu, K. *Phys. Rev. B* **2000**, *61*, 2188–2198.